ACS APPLIED MATERIALS & INTERFACES

RESEARCH ARTICLE

www.acsami.org

Charge Injection Engineering of Ambipolar Field-Effect Transistors for High-Performance Organic Complementary Circuits

Kang-Jun Baeg,[*,†] Juhwan Kim,[‡] Dongyoon Khim,[‡] Mario Caironi,[§] Dong-Yu Kim,[*,‡] In-Kyu You,[†] Jordan R. Quinn,[∥] Antonio Facchetti,[*,∥] and Yong-Young Noh[*,⊥]

[⊥]Department of Chemical Engineering, Hanbat National University, San 16-1, Dukmyung-dong, Yuseong-gu, Daejeon 305-719, Republic of Korea

[†]Convergence Components and Materials Research Laboratory, Electronics and Telecommunications Research Institute (ETRI), 218 Gajeongno, Yuseong-gu, Daejeon 305-700, Republic of Korea

[‡]Heeger Center for Advanced Materials, Department of Materials Science and Engineering, Gwangju Institute of Science and Technology (GIST), 261 Cheomdan-gwagiro, Buk-gu, Gwangju 500-712, Republic of Korea

[§]Center for Nano Science and Technology @Polimi, Istituto Italiano di Tecnologia, Via Pascoli 70/3, 20133 Milano, Italy

[∥]Polyera Corporation, 8045 Lamon Avenue Skokie, Ilinois 60077, United States

Supporting Information

ABSTRACT: Ambipolar π-conjugated polymers may provide inexpensive large-area manufacturing of complementary integrated circuits (CICs) without requiring micro-patterning of the individual p- and n-channel semiconductors. However, current-generation ambipolar semiconductor-based CICs suffer from higher static power consumption, low operation frequencies, and degraded noise margins compared to complementary logics based on unipolar p- and n-channel organic field-effect transistors (OFETs). Here, we demonstrate a simple methodology to control charge injection and transport in ambipolar OFETs via engineering of the electrical contacts. Solution-processed caesium (Cs) salts, as electron-injection and hole-blocking layers at the interface between semiconductors and charge injection electrodes, significantly decrease the gold (Au) work function (~4.1 eV) compared to that of a pristine Au electrode (~4.7 eV). By controlling the electrode surface chemistry, excellent p-channel (hole mobility ~0.1−0.6 $cm^2/(Vs)$) and n-channel (electron mobility ~0.1−0.3 $cm^2/(Vs)$) OFET characteristics with the same semiconductor are demonstrated. Most importantly, in these OFETs the counterpart charge carrier currents are highly suppressed for depletion mode operation (I_{off} < 70 nA when I_{on} > 0.1−0.2 mA). Thus, high-performance, truly complementary inverters (high gain >50 and high noise margin >75% of ideal value) and ring oscillators (oscillation frequency ~12 kHz) based on a solution-processed ambipolar polymer are demonstrated.

KEYWORDS: ambipolarity, polymer semiconductor, charge injection, caesium salts, complementary circuit, ring oscillator

INTRODUCTION

To satisfy the forecasted demand for organic integrated circuits (ICs) for applications such as logic circuits in printed radio-frequency identification tags, memories, sensors, and display drivers, the maximum operational frequency should be markedly improved compared to present technologies.[1−3] IC speeds are mainly determined by the field-effect mobility (μ_{FET}) of the semiconductors, which must be maximized through new semiconductor design and/or morphology optimization,[4−8] the circuit architecture (e.g., unipolar or complementary), the transistor dimensions,[9] and the parasitic resistance and capacitance.[10,11] Therefore, to enhance IC performance, it is necessary to first develop down-scaled organic field-effect transistors (OFETs) with high μ_{FET} and low parasitic characteristics.[12] Furthermore, these ICs must have a complementary circuit architecture consisting of p- and n-channel transistors to enable minimum transition delays, high noise immunity, and negligible power consumption in the static states.[10] Solution-processed complementary ring oscillators (ROs), in which the p- and n-channel FETs are patterned by a variety of printing techniques, can enable the development of extremely low-cost ICs. Although there have been a few extraordinary studies with high speeds above 100 kHz,[13,14] printed organic ROs have typically shown relatively lower oscillation frequencies (f_{osc}) than vapor-deposited organic circuits,[15−21] because of the relatively low μ_{FET} of solution-processed organic semiconductors, the large channel dimension, and the typically unipolar circuit architecture.

Solution-processable ambipolar semiconductors are of interest for use in complementary-like organic ICs. These circuits can be fabricated more easily than those based on p- and n-channel semiconductors since the ambipolar material can be deposited without the need of micro-patterning of the individual p- and n-type FETs.[22−25] Ambipolar transistors are achieved by using a single semiconductor, a semiconductor blend, or a multi-layer semiconductor film.[26−30] Obviously, a single-component semiconductor layer would be the best choice for facile IC fabrication. However, this approach requires efficient injection (and transport) of both charge carriers into a particular semiconductor

Received: June 1, 2011
Accepted: July 18, 2011
Published: August 01, 2011

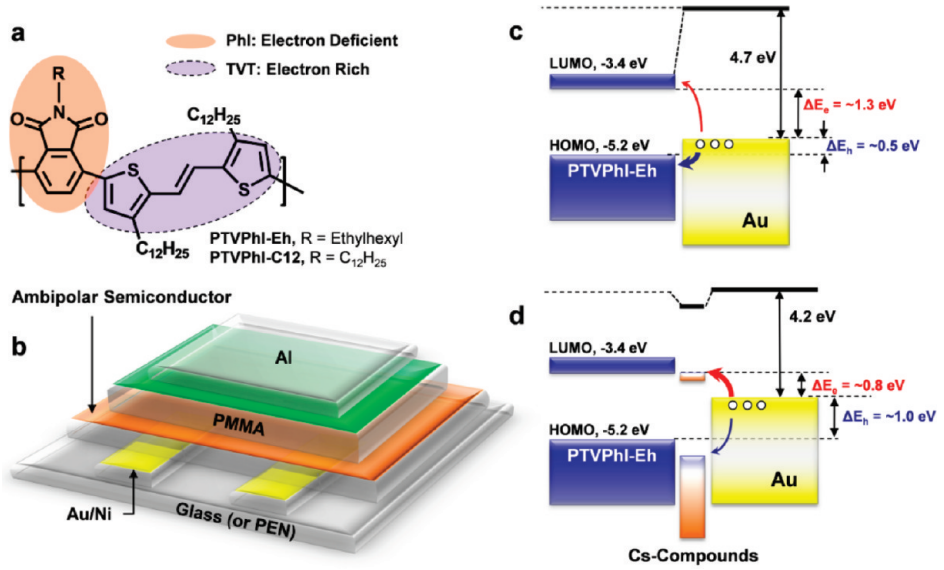

Figure 1. (a) Molecular structure of the PTVPhI-Eh and -C12; (b) TG/BC OFET device structure; (c) energy level alignment of an organic semiconductor on a pristine Au S/D electrode; and (d) after incorporation of the CILs between the organic semiconductor and Au.

from a single electrode, typically gold (Au), which is a major obstacle because most common organic semiconductors for FETs have a band gap of 2−3 eV.[31] Recently, a variety of low-band-gap conjugated polymers have been developed based on alternating electron donor−acceptor units in the polymer backbone.[32] These so-called push-pull copolymers, consisting of electron-rich and electron-deficient moieties, are coupled to reduce the bond length alternation and thus the band gap.[33] Among them, 1,4-diketopyrrolo[3,4-c]pyrrole-based copolymers have shown impressive carrier mobilities for both electrons ($\mu_e \approx 0.1$ cm^2/(V s)) and holes ($\mu_h \approx 0.65$ cm^2/(V s)),[34] which are close to those of the state-of-the-art unipolar conjugated polymers.[35,36] Although these ambipolar semiconductors exhibit high carrier mobilities, some obstacles remain to their adoption in commercially relevant printed ICs, mainly because neither OFET can be fully switched off in a complementary-like architecture. The associated leakage currents would increase the static power consumption and decrease the noise margins, and therefore the robustness to noise and parameter scattering, compared to complementary logic based on unipolar p-/n-type transistors. Here we report a simple methodology to selectively control charge injection in ambipolar OFETs enabling high-performance ICs by the insertion of a thin caesium carbonate (Cs_2CO_3) or caesium fluoride (CsF) film as an electron-injection/hole-blocking layer (hereafter referred to as charge injection layer, CIL) at the semiconductor-Au electrode interface. This methodology demonstrates the first selective deposition of the contact interlayer onto the n-type IC regions via thermal evaporation or a simple spray printing process, thus enabling the high-performance complementary inverters (gain >50) and ring oscillators ($f_{osc} \sim 12$ kHz) based on ambipolar polymers.

RESULTS AND DISCUSSION

Semiconductor Material Selection, Transistor Fabrication, and Measurements. Two newly developed donor−acceptor co-polymers, poly(thienylenevinylene-co- phthalimide)s functionalized at the imide nitrogen with 2-ethylhexyl (PTVPhI-Eh) and -dodecyl (PTVPhI-C12) chains, were used in this study to demonstrate our methodology. The molecular structure of these co-polymers consists of an electron-rich TV unit and an electron-deficient PhI moiety, promoting ambipolarity (Figure 1a). The long alkyl side chains, -Eh and -C12, enable solution-processability and enhance the thin-film order by side chain interactions. PTVPhI-Eh and -C12 have similar lowest unoccupied molecular orbitals (LUMO) and highest occupied molecular orbitals (HOMO) of −3.5 and −5.2 eV, respectively. The charge-transport properties of these polymers were measured in top-gate/bottom-contact (TG/BC) devices (Figure 1b). Briefly, these OFETs were fabricated on glass substrates consisting of Au (or Au-CIL) contacts, a spin-coated semiconductor layer, a poly(methyl methacrylate) (PMMA) dielectric layer, and a top aluminium (Al) gate electrode (see Experimental Section). All relevant FET parameters are reported in Table 1 and Table S1 in the Supporting Information.

The OFETs based on the PTVPhI polymers with Au contacts exhibited pronounced hole-transport ($\mu_h \approx 0.1 - 0.6$ cm^2/(V s), on/off current ratio $I_{on}/I_{off} \approx 1 \times 10^5$, $V_{Th,h} \approx -40$ to -47 V at $V_d = -80$ V), but lower electron-transport ($\mu_e \approx 0.01-0.02$ cm^2/(V s), $I_{on}/I_{off} \sim 1 \times 10^2$, $V_{Th,e} \approx 55-62$ V at $V_d = 80$ V) characteristics. Moreover, both the threshold voltage (V_{Th}) and the onset voltage (V_{on}) are much larger when these OFETs were measured for n-type operation (Figure 2 and Table 1). This effect is attributed to the energy level mismatch for electron and hole injection between the semiconductor frontier molecular orbital and the Au electrode (Figure 1c,d). The work function of the bottom-contact Au electrode typically decreases to −4.4 to −4.7 eV compared to that of the atomically clean Au surface (ca. −5.1 eV), due to interface dipole formation.[37,38] The main contribution to the interface dipole arises from the "push-back" effect due to the compression of the metallic electron density tail in the presence of an adsorbed organic layer.[38] Although the interface dipole typically favors electron injection by lowering the metal work function, the energy barrier for electron injection in our systems ($\Delta E_e \approx 1.2$ eV) was much higher than that of hole injection ($\Delta E_h \approx 0.5$ eV).

Table 1. Fundamental Parameters of the TG/BC OFETs Based on PTVPhI-Derivatives and P2100 before and after Deposition (by spin-coating) of Cs_2CO_3 and CsF Layers onto Au S/D Electrodes*

		p-channel			n-channel		
OSC	CIL	μ_h ($cm^2/(V\,s)$)	$V_{Th,h}$ (V)	$V_{On,h}$ (V)	μ_e ($cm^2/(V\,s)$)	$V_{Th,e}$ (V)	$V_{On,e}$ (V)
PTVPhI-Eh	none	0.54 (± 0.067)	−42.9 (± 2.17)	−8.9 (± 2.50)	0.022 (± 0.001)	61.1 (± 0.64)	58.2 (± 1.01)
	Cs_2CO_3	0.032 (± 0.014)	−56.8 (± 3.54)	−42.7 (± 2.10)	0.089 (± 0.006)	56.3 (± 5.07)	23.1 (± 3.14)
	CsF	0.040 (± 0.013)	−63.0 (± 2.15)	−48.4 (± 1.53)	0.26 (± 0.01)	44.27 (± 0.71)	24.7 (± 2.13)
PTVPhI-C12	none	0.067 (± 0.021)	−46.9 (± 0.40)	−15.7 (± 4.31)	0.010 (± 0.006)	52.3 (± 4.74)	52.1 (± 3.25)
	Cs_2CO_3	0.011 (± 0.020)	−66.1 (± 4.17)	−51.5 (± 4.10)	0.068 (± 0.018)	49.7 (± 5.01)	23.1 (± 4.32)
	CsF	0.028 (± 0.016)	-61.3 (± 3.35)	-42.3 (± 1.25)	0.10 (± 0.017)	49.9 (± 1.40)	29.2 (± 3.25)
ActivInk P2100	none	0.39 (± 0.021)	−21.1 (± 7.78)	6.8 (± 8.84)	0.002 (± 0.005)	61.9 (± 3.61)	21.0 (± 5.11)
	Cs_2CO_3	0.30 (± 0.02)	−38.2 (± 0.93)	−27.5 (± 1.62)	0.23 (± 0.01)	60.0 (± 0.49)	50.4 (± 0.59)
	CsF	0.35 (± 0.042)	−37.0 (± 2.47)	−26.1 (± 1.19)	0.13 (± 0.061)	53.2 (± 4.97)	18.9 (± 6.27)

*The field-effect mobility (μ_{FET}) and the threshold voltage (V_{Th}) were calculated at the saturation region (V_d = ±80 V) using gradual channel approximations equations. (W/L = 1.0 mm/20μm, PMMA gate dielectric thickness and capacitance were ~520 nm and ~6.0 nF/cm^2).

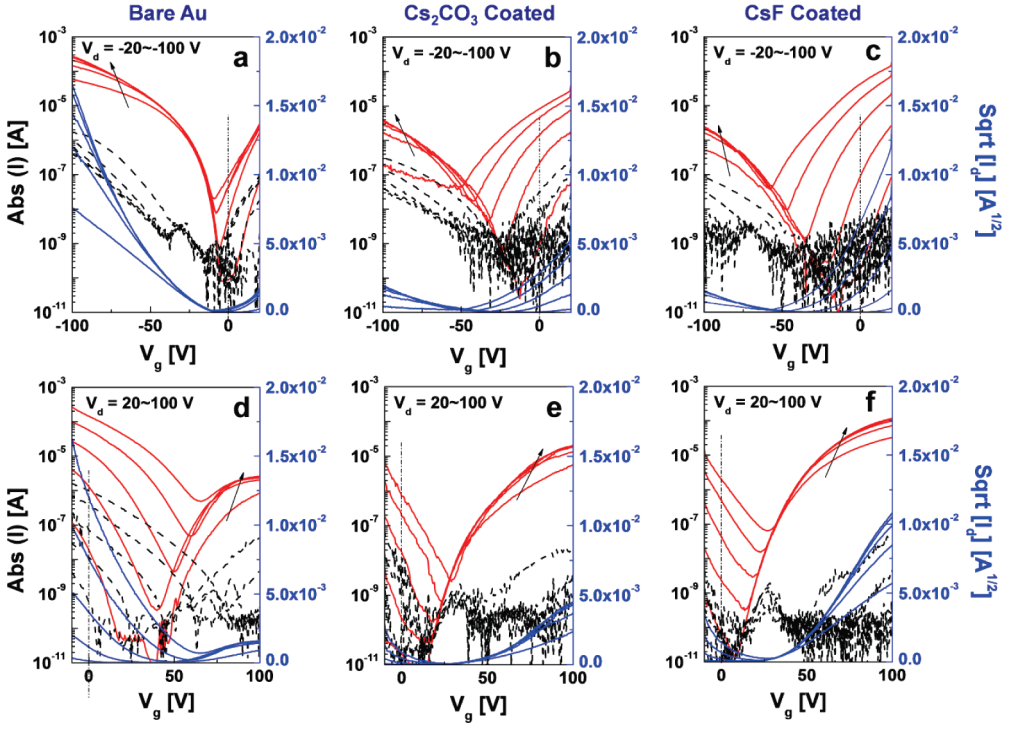

Figure 2. Transfer characteristics of the ambipolar OFETs based on PTVPhI-Eh at the (a−c) p-channel and (d−f) n-channel regions. (a, d) Before incorporation of the charge injection layers, and after spin-coating of (b, e) Cs_2CO_3 and (c, f) CsF onto bare Au S/D electrodes. (Solid red lines, Abs(I_d); solid blue lines, sqrt(I_d); and dotted black lines, I_g).

Therefore, pristine Au-based PTVPhI-Eh devices exhibited dominant p-channel OFET characteristics.

Charge Injection Layer Modification of Electrical Contacts and Implications for Transistor Performance. The n-channel characteristics of PTVPhI-Eh and -C12 OFETs can be significantly improved by the incorporation of nano-scale CILs derived from either Cs_2CO_3 or CsF. These inexpensive and commercially available Cs salts are soluble in alcohols, such as 2-ethoxyethanol, and can be spin- or spray-coated onto the Au electrodes before semiconductor deposition. As shown in Figure 3, the solution-deposited Cs_2CO_3 and CsF layers form discrete domains, mostly consisting of the pristine salts and not of metallic Cs or Cs-suboxide species as accessed by X-ray photoelectron spectroscopy measurements (Figure 4). Solution-processed Cs salts are not as prone to decomposition.[39] The transfer curves of Au-CIL-modified OFETs demonstrated remarkably improved n-channel characteristics (see Figure 2). The μ_e increased by >10×, reaching 0.27 $cm^2/(V\,s)$ and 0.12 $cm^2/(V\,s)$ for PTVPhI-Eh and -C12, respectively, while V_{Th} and V_{on} showed a significant reduction ($\Delta V_{Th} \approx 16.9$ V and $\Delta V_{on} \approx 33.5$ V for PTVPhI-Eh). The performance of these n-channel FETs is comparable to that of state-of-the-art n-type polymers.[36] To understand the origin of the performance variations, the semiconductor film morphology was investigated by atomic force microscopy (AFM). For instance, the

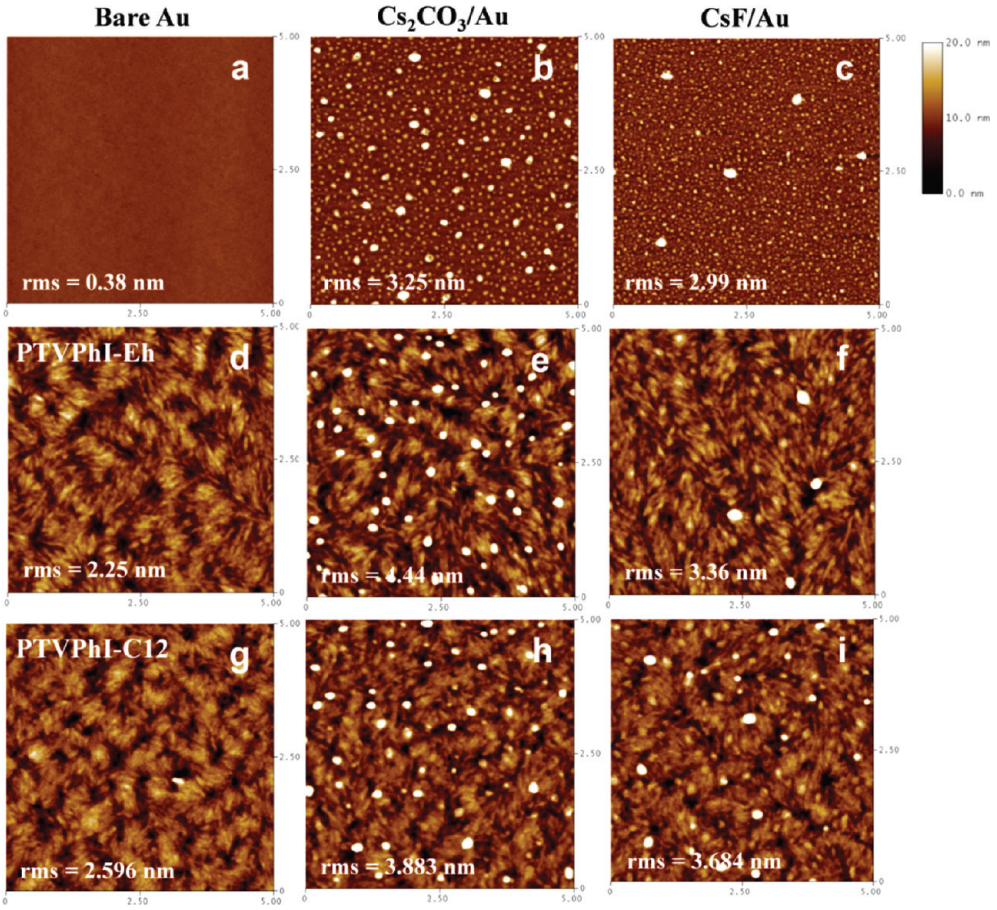

Figure 3. Tapping mode AFM images. (a) Pristine Au surface, (b) Cs_2CO_3-coated, and (c) CsF-coated Au surfaces. PTVPhI-Eh surface images (d) on pristine Au, and with (e) Cs_2CO_3-coated and (f) CsF-coated Au. PTVPhI-C12 surface images (g) on pristine Au, and with (h) Cs_2CO_3-coated and (i) CsF-coated Au. (rms: root mean square roughness).

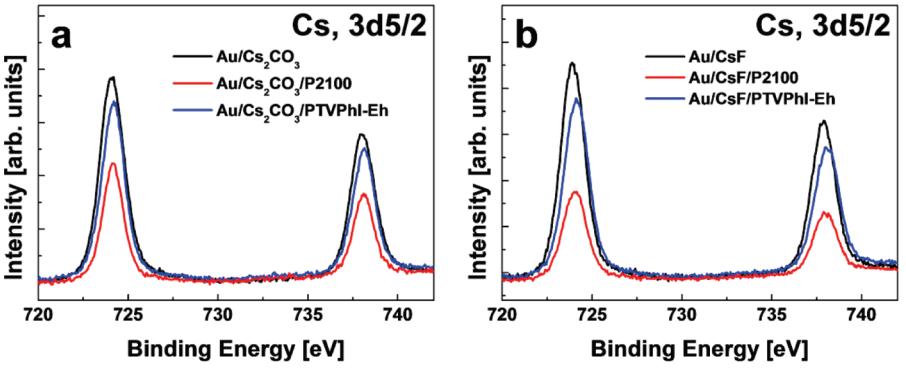

Figure 4. XPS profiles of the spin-coated Cs_2CO_3 and CsF films on Au contacts. Detailed Cs 3d spectra of the (a) Cs_2CO_3- and (b) CsF-deposited films. P2100 and PTVPhI-Eh films were spin-coated onto the Cs_2CO_3 and CsF film, respectively.

PTVPhI-Eh films on pristine Au showed a highly ordered fibril-like morphology (see Figure 3d), and no significant morphological changes were observed for the same films on Au-CIL surfaces (Figure 3e,f). Therefore, the dramatic changes in the transistor characteristics are not morphological in origin; rather, they are the result of electronic modification of the semiconductor−electrode interface by the insertion of the CILs.

To clarify this essential point, we measured the Au electrode work function (ϕ) by Kelvin probe force measurements and was found to decrease from −4.7 eV to −4.1 to −4.2 eV after CIL deposition. Very thin or nanostructured Cs_2CO_3 and CsF interlayers are well known for their ability to improve electron injection of several metal cathodes in organic optoelectronic devices by ∼0.5−1.5 eV, depending on the deposition method.[39−42] Thus, a similar effect should take place in our devices, where the formation of Au−O−Cs or Au−F−Cs complexes lowered the Au work function and consequently decreased ΔE_e by ∼0.7 eV. In contrast, to favor electron

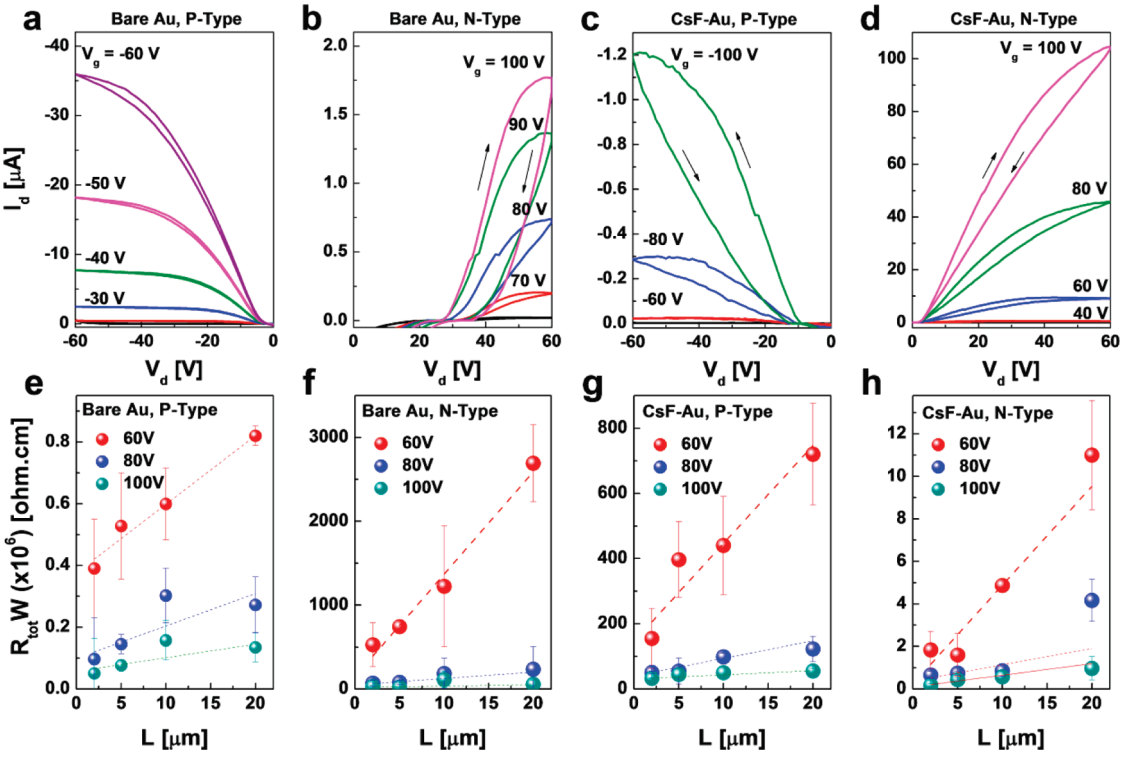

Figure 5. Output characteristics of the ambipolar OFETs based on PTVPhI-Eh for (a, c) p-channel and (b, d) n-channel operation [W/L = 1.0 mm/20 μm]. Output characteristics on (a, b) bare Au contacts and (c, d) after spin-coating CsF CIL on the electrodes. Total resistance (R_{tot}) of the ambipolar OFETs based on PTVPhI-Eh for (e, g) p-channel and (f, h) n-channel operation [W = 1.0 mm and L = 2, 5, 10, and 20 μm] at V_g = 40, 60, 80, and 100 V. Output characteristics on (e, f) bare Au contacts and (g, h) after spin-coating CsF CIL on the electrodes. R_c values were obtained using the transfer line method.

injection, the decreased ϕ of the Au-CIL electrode reduced hole injection and degraded FET characteristics with $\mu_h \approx 0.03-0.05$ cm^2/(V s), $I_{on}/I_{off} \approx 1 \times 10^2$, and $V_{Th,h} \approx -55$ to -65 V for PTVPhI-Eh and μ_h 0.01$-$0.03 cm^2/(V s), $I_{on}/I_{off} \approx 1 \times 10^2$, and $V_{Th,h} \approx -60$ to -70 V for PTVPhI-C12. Quantitative information on FET contact resistance (R_c) variation upon electrode functionalization was extracted from the $I-V$ output plots in the case of PTVPhI-Eh OFETs. For the CIL-based devices, the $I-V$ curves clearly exhibited reduced nonlinearity at low V_d, and thus lower R_c, for n-channel operation (see Figure 5), whereas the opposite behaviour was observed for p-channel operation. The R_c was measured using the transmission line method[43] at $V_g = \pm 80$ V (Figure 5e$-$h). The pristine Au-based PTVPhI-Eh devices exhibited significantly lower R_c for the p-channel ($\sim 1.0 \pm 0.4 \times 10^5$ Ωcm) than for the n-channel ($\sim 4.7 \pm 1.5 \times 10^7$ Ωcm) device operation. In contrast, for Au-CIL devices, R_c decreased by >100$\times$ for electron injection ($\sim 3.7 \pm 3.3 \times 10^5$ Ωcm), whereas it increased for hole injection ($\sim 3.9 \pm 2.9 \times 10^7$ Ωcm). The key role of R_c in tuning the performances of these ambipolar OFETs is, therefore, evident.

To broaden the scope and applicability of this methodology, enhance n-channel performance for low band-gap materials via CIL functionalization, and make a direct comparison with previously demonstrated all-polymer ICs,[44] we also utilized a commercially available high-performance semiconductor (Activ-Ink P2100). We recently demonstrated high-speed organic ROs ($\sim$50 kHz) based on individually inkjet-patterned P2100 (p-type) and poly{[N,N′-bis(2-octyldodecyl)-naphthalene-1,4,5,8-bis(dicarboximide)-2,6-diyl]-alt-5,5′-(2,2′-dithiophene)} (P(NDI2OD-T2), n-type) transistors.[44] As shown in Figure S2 in the Supporting Information, the Au-based P2100 OFETs exhibited unbalanced p- and n-type characteristics, in which μ_h was considerably larger ($\sim$0.4 cm^2/(V s)) than μ_e ($\sim$0.002 cm^2/(V s)). However, the n-channel characteristics of P2100 OFETs also improved remarkably after insertion of the CILs (Cs_2CO_3 and CsF). The μ_e increased by 100$\times$ ($\sim$0.2 cm^2/(V s)). It is interesting that, unlike the PTVPhI-based polymers, the interlayer-modified P2100 devices retained excellent hole transport with μ_h $\sim$0.3$-$0.4 cm^2/(V s). This result can be attributed to a relatively lower band gap ($\sim$1.6 eV) and HOMO energy level ($-$4.92 eV) of the P2100, compared to the PTVPhI-based polymers (see Figure S1 in the Supporting Information).

All of the CIL-modified ambipolar transistors measured in the present study exhibited comparable device characteristic variations upon CIL insertion, independent of the CIL deposition method (spin-coating, spray-printing, or thermal evaporation, see Figure 6 and Figure S5 in the Supporting Information). However, FET characteristics significantly depended on the spray or thermal evaporation deposition time, and thus, the Au surface coverage and the CIL film thickness. Figure 6 shows that the initial performance of the p-channel transistors gradually decreased as the spray time increased. On the other hand, the n-channel FET properties first showed an enhancement with increasing spraying time up to 6 s, followed by a degradation of the n-type performance as the result of the thicker, more insulating CIL film. The Au ϕ showed a similar trend, characterized by a rapid decrease as the spray time increased then saturated at $-$4.1 to $-$4.2 eV. It is worth noting that n-type doping could

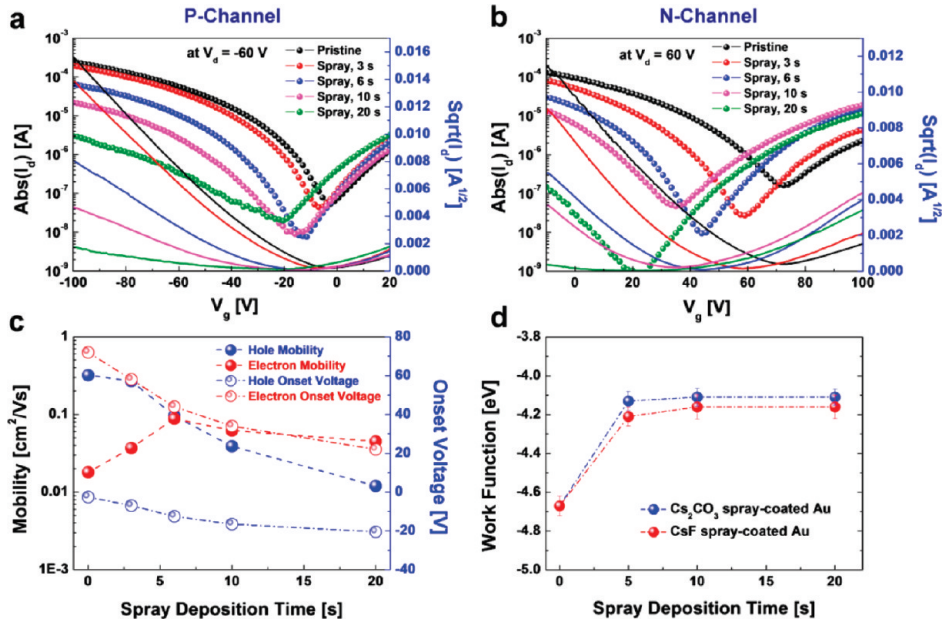

Figure 6. Transfer characteristics of OFETs based on P2100 as a function of Cs_2CO_3 spray deposition time (from 3 to 20 s). (a) At $V_d = -60$ V (p-channel) and (b) at $V_d = 60$ V (n-channel) ($W/L = 1.0$ mm/20μm). (c) The corresponding electron and hole mobilities and onset voltage variations as a function of the Cs_2CO_3 spray deposition time. (d) Au work-function variations, measured by kelvin probe force microscopy, as a function of CsF and Cs_2CO_3 spray deposition time.

also take place at the semiconductor/dielectric interface,[45−47] although we still have no evidence from the XPS and UV/VIS/NIR absorption spectra (Figure 4 and Figure S1 in the Supporting Information). The Cs salts are known as strong n-type dopants with organic semiconductors,[45] in which trap-free electron transport is enabled by the application of n-type doping to inactivate the deep trap states.[47]

Complementary Circuits Based on Ambipolar Semiconductors. Although a few research groups have reported excellent complementary-like inverters based on ambipolar FETs,[48−50] these transistors cannot be used in complex digital or analogue circuits. Even an excellent ambipolar device, with balanced μ_e and μ_h and both $V_{Th,e}$ and $V_{Th,h}$ ~0 V, would not enable the key characteristics of a complementary circuit, low static power consumption and large noise margins, due to typical a Z-shaped voltage transfer characteristic (VTC).[48−50] Ambipolarity and complementarity are two antithetical aspects. A perfectly ambipolar device, with balanced μ_e and μ_h and both $V_{Th,e}$ and $V_{Th,h}$ close to 0 V, is not suitable for a complementary circuit configuration. In a complementary inverter (such as the one depicted in Figure 7d), the input voltage V_{in} alternatively switches on and off the p- and n-channel transistors, respectively, which are the pull-up and pull-down transistor. When V_{in} is low, the pull-down, n-type FET is off and behaves like a high impedance load, while the pull-up, p-type FET is on and drives the output to the high supply voltage; the opposite is true when V_{in} is high. If both devices are at the same time good p- and n-type transistors this configuration would fail. Indeed it is possible to obtain an inverting VTC even with balanced ambipolar devices. However, the presence of a parallel, parasitic p-channel (n-channel) that switches on in the pull-down (pull-up) FET when the n-channel (p-channel) is switched off, reduces the impedance of the transistor acting as the load, thus strongly reducing the output voltage swing. This effect produces the typical Z-shaped VTC, resulting in high static power consumption and very limited noise margins compared to conventional complementary logic inverters. Therefore, to enable complementary logic based on ambipolar polymers, it is crucial to reduce the leakage current in the off state by suppressing the current as much as possible in the parallel counterpart transistor.

Therefore, to benefit from ambipolar polymer-based complementary logic, it is crucial to achieve excellent unipolar transistor operation in which the "parasitic" currents are suppressed. Thus, when operating the device in the p- (n-) channel mode the device currents for positive (negative) biases should be as low as possible. As shown in Figure 7c, the complementary inverter based on the ambipolar PTVPhI-Eh OFETs and bare Au contacts exhibited Z-shape-like VTC curves, and very narrow noise margins of ~33 and ~20% of 1/2 V_{DD} at low (NM_L) and high levels (NM_H), respectively. The output voltage (V_{out}) deviated from the supply voltage (V_{DD}) for low input voltages (V_{in}) due to the efficient hole transport in the pull-down transistor, with a W that was 5× larger, thus strongly reducing its impedance. For larger V_{in}, the VTC curves did not exhibit the typical Z-shape observed in a very well-balanced ambipolar inverter. This was attributed to low n-channel conductivity; the "n-type" pull-down FET did not have sufficient current to drive the output completely to ground, and the parasitic n-channel current of the pull-up transistor was not large enough to affect the V_{out} due to a smaller W (Figure 7b). The V_{out} loss at $V_{DD} = +100$ V was as high as +45 V and +12 V for $V_{in} = 0$ V and +80 V, respectively.

To enable truly complementary logic based on a single semiconductor, CIL-modified contacts were used to selectively improve the n-channel characteristics of PTVPhI-Eh-based FETs. Spray-printing was used to deposit the CILs onto the n-channel region of the IC. This method is far simpler and can be readily used for the fabrication of IC over a large area, versus sophisticated micro-patterning of both types of semiconductors.[44] After selective deposition of the CsF layer onto the n-channel region, the

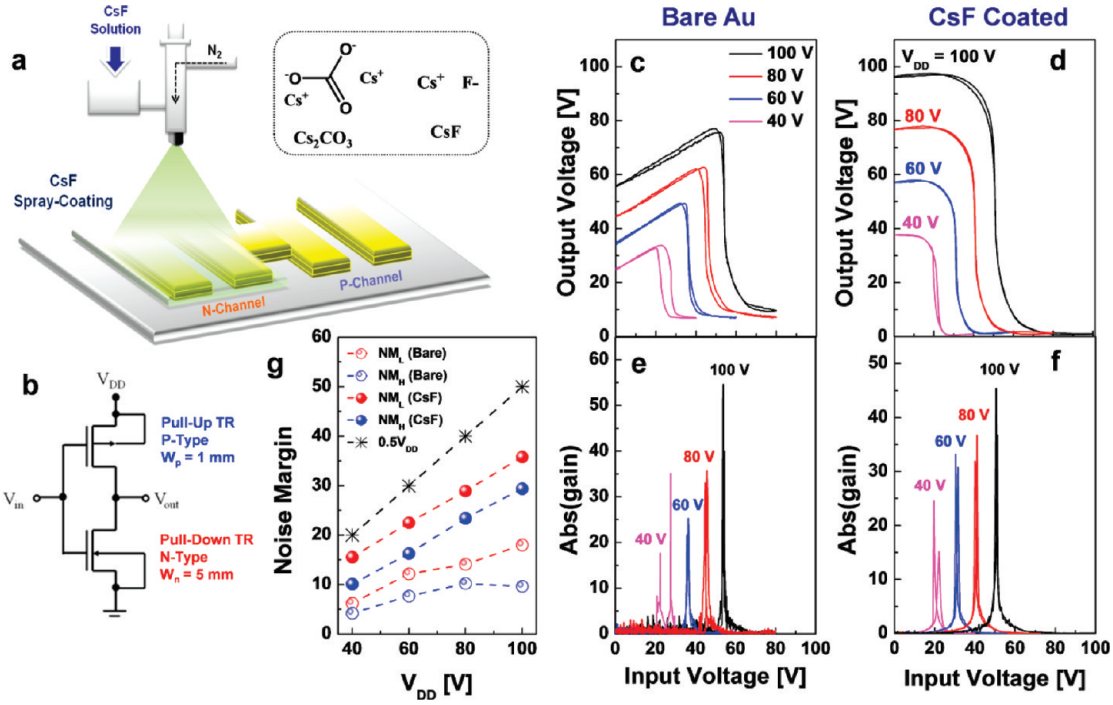

Figure 7. Complementary inverter circuits based on ambipolar PTVPhI-Eh OFETs [W/L ratios for p-channel, W_p/L_p = 1 mm/20 μm, and for n-channel, W_n/L_n = 5 mm/20 μm]. (a) Molecular structure of Cs_2CO_3 and CsF, and schematic illustration of the spray-coating process, where Cs_2CO_3 and CsF were deposited selectively onto the n-channel transistor region. (b) Circuit configuration of the complementary inverter. Voltage transfer characteristics and corresponding output voltage gains of the inverters: (c, e) bare Au S/D electrode; and, (d, f) after selective spray-deposited CsF layer. (g) Noise margins of the corresponding inverter with or without the CsF layer only in the n-channel region.

complementary inverter based on PTVPhI-Eh exhibited excellent VTC curves (Figure 7d) with text-book complementary metal-oxide-semiconductor inverter behaviour.[10] V_{out} loss markedly decreased to <+4 V in the static off-state (V_{in} = 0 V) and was negligible in the on-state (V_{in} = +80 V), due to a suppressed hole-current at V_{in} = 0 V and an enhanced electron-current at V_{in} = +80 V in the n-channel pull-down transistor. Similar characteristics were observed for the PTVPhI-12-based ICs. These complementary inverters exhibited a very high voltage gain of >50 (at V_{DD} = +100 V), a negligible bias hysteresis, and good noise margins as high as ~75% of 1/2 V_{DD} (see Figure 7d, f,g).[51] As shown in Figure S7 in the Supporting Information, the inverting voltage (V_{inv}) shifted to ~11.5 V approaching 1/2 V_{DD}, and the V_{out} loss in both static on- and off-states gradually decreased as the W/L ratios of the n-channel transistors increased. In complementary inverters after incorporation of the CsF, significant power was only consumed during the switching process (maximum ~1 mW at V_{in} = V_{inv}), and showed more than 10× lower power consumption at the static states, V_{in} = 0 V and V_{DD} = 100 V, of ~0.1 mW vs ~1 mW without the CsF layer. Note that the VTC shape of P2100-based inverters did not improve substantially when CIL-modified contacts were used for the n-channel FETs (V_{out} loss ~30 V, see Figure S8 in the Supporting Information), due to the presence of a conductive p-channel in the pull-down FET (see Figure S2 in the Supporting Information).

Complementary ROs were also demonstrated (L_n = L_p = 10 μm; W_n = W_p = 10 mm) for an accurate analysis of the IC dynamic switching characteristics (Figure 8). These devices were fabricated with and without spin- or selective spray coating of CsF onto the Au electrode n-channel (pull-down) transistor region. Next, the PTVPhI-Eh and dielectric PMMA films were deposited by spin-coating, followed by via-hole definition accomplished by removing part of the dielectric and semiconductor layers by inkjet printing of chlorobenzene.[44] Finally, the gate was deposited by thermal evaporation of Al. Figure 8c shows that the bare Au-based RO did not oscillate for $|V_{DD}|$ < 140 V, and very low frequencies (~0.2 kHz) were measured for larger V_{DD}. When the CIL was blanket spin-coated on the n-channel FET contacts, the pull-down n-channel property improved more than 10×, while simultaneously, the reduced pull-up p-channel characteristics continued to cause a slow f_{osc} of 0.84 kHz at $|V_{DD}|$ = 160 V. The maximum f_{osc}, as high as 12 kHz, was achieved by selective deposition of the CsF layer onto the n-channel transistor region by spray printing. The V_{DD} to induce RO voltage was significantly reduced from +140 V (bare Au) to +80 V (spray CsF), because of the decreased $V_{Th,e}$ (~17 V) after CIL incorporation. Note that the use of thinner or higher-k dielectrics can reduce the high V_{DD} that is used here (80−160 V). Such a high-speed ambipolar polymer RO can be achieved by a combination of pull-up transistors with pristine Au S/D electrodes ($\mu_h \approx 0.61$ cm^2/(V s) and $V_{Th,h} \approx -42.9$ V) and pull-down transistors with spray-printed CsF on an Au S/D ($\mu_e \approx 0.27$ cm^2/(V s) and $V_{Th,e} \approx +44.2$ V) in a truly complementary inverter, and its sequential connection into the circuits.

The RO f_{osc} depends on the number of inverting gates (n) and on their propagation delay (τ), and can be determined by $f_{osc} = 1/(2n\tau)$. Because τ is the sum of the low-to-high output transition time driven by the pull-up (p-type) transistor on-current and the high-to-low transition time driven by the pull-down (n-type) transistor,[11] it is inversely proportional to μ_h, μ_e and V_{DD}. Therefore, f_{osc} increased proportionally with the

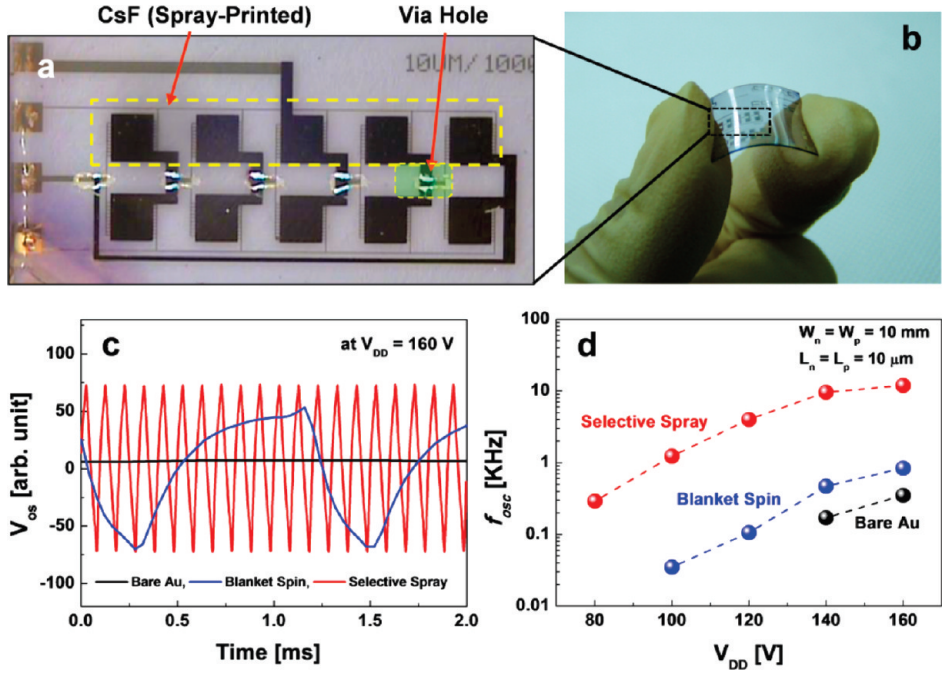

Figure 8. Complementary ring oscillators (RO) based on ambipolar PTVPhI-Eh OFETs [$L_n = L_p = 10\mu$m, and $W_n = W_p = 10$ mm]. (a) Optical microscope image of the RO circuit, and (b) digital camera image of flexible ambipolar polymer RO fabricated onto a plastic substrate (PEN, Tenjin Dupont); selective spray deposition area of the CsF (n-channel region) and via-hole are indicated in the figure. (c) Voltage oscillation (V_{os}) at $V_{DD} = 160$ V of the RO under various Au S/D electrode conditions; black line—bare Au, blue line—blanket spin-coated CsF, and red line—selective spray-printed CsF. (d) Dependence of the oscillation frequencies (f_{osc}) on the supply voltage (V_{DD}) in the 80 to 160 V range.

previous parameters (see Figure 8d). Note that the f_{osc} values reported here were comparable, given a similar device architecture and dielectric thickness, to our complementary circuits based on high-performance inkjet-patterned p- and n-type polymers FETs,[44] and, as far as we could ascertain, exhibited one of the best performance to date for ambipolar semiconductor-based devices. Finally, Figure 8b shows a flexible PTVPhI-Eh-based RO fabricated on a polyethylene naphthalate (PEN) substrate in which the CIL was spray-patterned. Remarkably, this device functioned similar to the one fabricated on glass with a f_{osc} of ~10 kHz at $|V_{DD}| = 160$ V.

CONCLUSIONS

In conclusion, we demonstrated high-performance ICs via selectively controlled charge injection in ambipolar OFETs. Insertion of a thin Cs_2CO_3 or CsF CIL between the Au contact and the ambipolar semiconductor by simple spray-coating profoundly modified the transistor performance. Truly complementary inverters and RO circuits were demonstrated by combining ambipolar OFETs in which bare Au and Au-CIL contacts were used for the p- and n-channel operation, respectively. Inverters, the basic building blocks of ICs, exhibited ideal behaviour characterized by very high voltage gains (> 50) and high noise margins (~75% of 1/2 V_{DD}). A 5-stage RO exhibited a relatively high $f_{osc} \approx 12$ kHz. Our study demonstrates that complementary OFETs and circuits based on ambipolar polymers may become an option for the fabrication of a variety of low-cost, large-area organic ICs.

EXPERIMENTAL METHODS

Field-Effect Transistor Fabrication. Corning Eagle 2000 glass or PEN (Teijin Dupont Films) substrates were cleaned sequentially in an ultrasonic bath with de-ionized water, acetone, and isopropanol for 10 min each. The Au/Ni (15 nm/3 nm thick) patterns used for the S/D electrodes were fabricated using a conventional lift-off photolithography procedure. Cs_2CO_3 and CsF were purchased from Aldrich and dissolved in 2-ethoxyethanol for use (2 mg/mL concentration). The CILs were deposited by thermal evaporation and either spin-coating under N_2 or, in air, spray-printing the Cs_2CO_3 or CsF solutions onto the Au patterned electrodes, followed by thermal annealing at 120 °C for 30 min under N_2. The ambipolar polymer semiconducting materials, PTVPhI-Eh and PTVPhI-C12, were synthesized in our laboratory (see the Supporting Information), and P2100 was supplied by Polyera Corporation and used as received. PTVPhI-Eh, -C12 and P2100 were dissolved in anhydrous chlorobenzene to obtain 10 mg/mL solutions. These solutions were then filtered with a 0.2 μm polytetrafluoroethylene syringe filter before deposition by spin-coating. The PTVPhI polymers and the P2100 films were thermally annealed at 110 and 150 °C for 30 min, respectively, to remove the residual solvents and induce an ordered crystalline phase in a glove box with a N_2 atmosphere. PMMA (Aldrich, $M_W = 120$ kD) was used as a dielectric material without further purification. PMMA (80 mg/mL) was dissolved in n-butylacetate, and the solution was filtered with a 0.2 μm PTFE syringe filter before spin-coating. After deposition, the devices were annealed at 80 °C for 2 h under N_2. The transistors were completed by deposition of the top-gate electrodes via thermal evaporation of Al (~30 nm thick) using a metal shadow mask.

Complementary Inverter and Ring Oscillator Fabrication. The electrical contacts (Au/Ni) of these devices were patterned using photo-lithography and consisted of individual FET electrodes having dimensions of $L = 10$ or 20 μm, and $W = 1$, 5, or 10 mm. Cs_2CO_3 and CsF were either blanket spin-coated or spray-printed with a metal shadow mask for selective patterning of the n-channel transistor regions. After sequential spin-coating and thermal annealing of the semiconductors and the PMMA gate dielectric layers, as described previously, chlorobenzene was inkjet-printed on the device to create via-holes.

Finally, the devices were completed by the deposition of the gate electrodes (Al, ~ 1 μm thick) using a metal shadow mask.

Thin Film and Device Characterisation. The surface morphology of the films was investigated via tapping-mode AFM (Nanoscope III, Veeco Instruments, Inc.). The contact potential difference (CPD) of each sample was detected by a Kelvin probe (KP 6500 Digital Kelvin probe, McAllister Technical Services, Co. Ltd) under air. The CPD was calibrated to highly ordered pyrolytic graphite at -4.58 ± 0.03 eV. UV−Vis absorption spectra were measured using a UV/VIS/NIR spectrophotometer (Lambda 750, Perkin−Elmer). Cyclic voltammetry was conducted using an Autolab PGSTAT 30 Potentiostat/Galvanostat in an acetonitrile solution with 0.1 M tetrabutylammonium perchlorate (Bu_4NClO_4) as the supporting electrolyte, indium tin oxide as the working electrode, a Pt wire as the counter electrode, and a Ag wire as the reference electrode at a scan rate of 50 mV/s. The XPS measurement was carried out using AXIS-NOVA (Kratos, Inc.) with a base pressure of 4.2×10^{-9} Torr. The FET electrical characteristics and the static characteristics of the complementary inverters were measured using a Keithley 4200-SCS in a N_2-filled glove box. The μ_{FET} and V_{Th} were calculated at the saturation region using gradual channel approximation equations.[52] The dynamic characteristics of the inverter and the input/output voltage signals for the ROs were measured using a pulsed $I-V$ setup with a built-in Keithley 4200 (dual-channel pulse generator and oscilloscope).

■ ASSOCIATED CONTENT

Supporting Information. Synthesis, cyclic voltammograms, optical absorption spectra, and related HOMO and LUMO energy levels of ambipolar semiconductor materials, transfer characteristics of the ambipolar OFETs based on P2100, AFM image of the P2100 surface, electron and hole mobilities and corresponding V_{Th} as a function of V_d, transfer characteristics of PTVPhI OFETs with thermal deposited CsF layer, schematic illustration of the fabrication process for the ambipolar inverters and ring oscillators, voltage transfer characteristics at various V_{DD} and corresponding voltage gains of the complementary inverters based on PTVPhI-Eh and P2100 OFETs with different W/L ratios. This material is available free of charge via the Internet at http://pubs.acs.org/.

■ AUTHOR INFORMATION

Corresponding Authors

*E-mail: kangjun100@etri.re.kr (K.J.B); kimdy@gist.ac.kr (D.Y.K); afacchetti@polyera.com (A.F); yynoh@hanbat.ac.kr (Y.Y.N).

■ ACKNOWLEDGMENT

This research was financially supported for the development of printing ink for touch panels and OLED lighting (A2010DD006) funded by the Ministry of the Knowledge Economy (MKE), Daedeok Innopolis, the Basic Science Research Program through the National Research Foundation of Korea (NRF), funded by the Ministry of Education, Science and Technology (MEST) (2010-0023180), the development of new materials and solution processing for LCD backplanes by ISTK, the development of next generation RFID technology for item-level applications (2008-F052-01) funded by the Korean MKE, an NRF grant funded by the Korea government (MEST) (2010-0029212), the Program for Integrated Molecular Systems at GIST, the World Class University program through the Korea Science and Engineering Foundation funded by the MEST (R31-10026). Polyera thanks the FlexTech Alliance for supporting development of N2200.

■ REFERENCES

(1) Gelinck, G.; Heremans, P.; Nomoto, K.; Anthopoulos, T. D. *Adv. Mater.* **2010**, *22*, 3778–3798.
(2) Sakanoue, T.; Sirringhaus, H. *Nat. Mater.* **2010**, *9*, 736–740.
(3) Sekitani, T.; Zschieschang, U.; Klauk, H.; Someya, T. *Nat. Mater.* **2010**, *9*, 1015–1022.
(4) Klauk, H. *Chem. Soc. Rev.* **2010**, *39*, 2643–2666.
(5) Arias, A. C.; MacKenzie, J. D.; McCulloch, I.; Rivnay, J.; Salleo, A. *Chem. Rev.* **2010**, *110*, 3–24.
(6) Zhang, W.; Smith, J.; Watkins, S. E.; Gysel, R.; McGehee, M.; Salleo, A.; Kirkpatrick, J.; Ashraf, S.; Anthopoulos, T. D.; Heeney, M.; McCulloch, I. *J. Am. Chem. Soc.* **2010**, *132*, 11437–11439.
(7) Salleo, A.; Kline, R. J.; DeLongchamp, D. M.; Chabinyc, M. L. *Adv. Mater.* **2010**, *22*, 3812–3838.
(8) Rivnay, J.; Jimison, L. H.; Northrup, J. E.; Toney, M. F.; Noriega, R.; Lu, S.; Marks, T. J.; Facchetti, A.; Salleo, A. *Nat. Mater.* **2009**, *8*, 952–958.
(9) Caironi, M.; Gili, E.; Sakanoue, T.; Cheng, X.; Sirringhaus, H. *ACS Nano* **2010**, *4*, 1451–1456.
(10) Rabaey, J. M.; Chandrakasan, A.; Nikolić, B. *Digital Integrated Circuits*, 2nd ed.; Prentice Hall: Upper Saddle River, NJ, 2003.
(11) Sedra, A. S.; Smith, K. C. *Microelectronics Circuits*, 5th ed.; Oxford University Press: Cary, NC, 2003.
(12) Noh, Y.-Y.; Zhao, N.; Caironi, M.; Sirringhaus, H. *Nat. Nanotechnol.* **2007**, *2*, 784–789.
(13) Fix, W.; Ullmann, A.; Ficker, J.; Clemens, W. *Appl. Phys. Lett.* **2002**, *81*, 1735–1737.
(14) Knobloch, A.; Manuelli, A.; Bernds, A.; Clemens, W. *J. Appl. Phys.* **2004**, *96*, 2286–2291.
(15) Anthopoulos, T. D.; Singh, B.; Marjanovic, N.; Sariciftci, N. S.; Ramil, A. M.; Sitter, H.; Cölle, M.; de Leeuw, D. M. *Appl. Phys. Lett.* **2006**, *89*, 213504:1–3.
(16) Klauk, H.; Zschieschang, U.; Pflaum, J.; Halik, M. *Nature* **2007**, *445*, 745–748.
(17) Crone, B.; Dodabalapur, A.; Lin, Y.-Y.; Filas, R. W.; Bao, Z.; LaDuca, A.; Sarpeshkar, R.; Katz, H. E.; Li, W. *Nature* **2000**, *403*, 521–523.
(18) Cho, J. H.; Lee, J.; Xia, Y.; Kim, B.; He, Y.; Renn, M. J.; Lodge, T. P.; Frisbie, C. D. *Nat. Mater.* **2008**, *7*, 900–906.
(19) Yan, H.; Zheng, Y.; Blache, R.; Newman, C.; Lu, S.; Woerle, J.; Facchetti, A. *Adv. Mater.* **2008**, *20*, 3393–3398.
(20) Stingelin-Stutzmann, N.; Smits, E.; Wondergem, H.; Tanase, C.; Blom, P.; Smith, P.; de Leeuw, D. *Nat. Mater.* **2005**, *4*, 601–606.
(21) Yoo, B.; Jones, B. A.; Basu, D.; Fine, D.; Jung, T.; Mohapatra, S.; Facchetti, A.; Dimmler, K.; Wasielewski, M. R.; Marks, T. J.; Dodabalapur, A. *Adv. Mater.* **2007**, *19*, 4028–4032.
(22) Chen, Z.; Lemke, H.; Albert-Seifried, S.; Caironi, M.; Nielsen, M. M.; Heeney, M.; Zhang, W.; McCulloch, I.; Sirringhaus, H. *Adv. Mater.* **2010**, *22*, 2371–2375.
(23) Anthopoulos, T. D.; de Leeuw, D. M.; Cantatore, E.; Setayesh, S.; Meijer, E. J.; Tanase, C.; Hummelen, J. C.; Blom, P. W. M. *Appl. Phys. Lett.* **2004**, *85*, 4205–4207.
(24) Anthopoulos, T. D.; de Leeuw, D. M.; Cantatore, E.; van 't Hof, P.; Alma, J.; Hummelen, J. C. *J. Appl. Phys.* **2005**, *98*, 054503:1–6.
(25) Anthopoulos, T. D.; Setayesh, S.; Smits, E.; Cölle, M.; Cantatore, E.; de Boer, B.; Blom, P.W. M.; de Leeuw, D. M. *Adv. Mater.* **2006**, *18*, 1900–1904.
(26) Zaumseil, J.; Sirringhaus, H. *Chem. Rev.* **2007**, *107*, 1296–1323.
(27) Capelli, R.; Dinelli, F.; Toffanin, S.; Todescato, F.; Murgia, M.; Muccini, M.; Facchetti, A.; Marks, T. J. *J. Phys. Chem. C* **2008**, *112*, 12993–12999.
(28) Muccini, M. *Nat. Mater.* **2006**, *5*, 605–613.
(29) Dinelli, F. *Adv. Mater.* **2006**, *18*, 1416–1420.
(30) Capelli, R.; Toffanin, S.; Generali, G.; Usta, H.; Facchetti, A.; Muccini, M. *Nat. Mater.* **2010**, *9*, 496–503.
(31) Zaumseil, J. Ph.D. Thesis, University of Cambridge, U.K., 2007.
(32) Facchetti, A. *Chem. Mater.* **2011**, *23*, 733–758.

(33) Colladet, K.; Fourier, S.; Cleij, T. J.; Lutsen, L.; Gelan, J.; Vanderzande, D. *Macromolecules* **2007**, *40*, 65–72.
(34) Ashraf, R. S.; Chen, Z.; Leem, D. S.; Bronstein, H.; Zhang, W.; Schroeder, B.; Geerts, Y.; Smith, J.; Watkins, S.; Anthopoulos, T. D.; Sirringhaus, H.; de Mello, J. C.; Heeney, M.; McCulloch, I. *Chem. Mater.* **2011**, *23*, 768–770.
(35) Li, Y.; Singh, S. P.; Sonar, P. A. *Adv. Mater.* **2010**, *22*, 4862–4866.
(36) Yan, H.; Chen, Z.; Zheng, Y.; Newman, C.; Quinn, J. R.; Dötz, F.; Kastler, M.; Facchetti, A. *Nature* **2009**, *457*, 679–686.
(37) Braun, S.; Salaneck, W. R.; Fahlman, M. *Adv. Mater.* **2009**, *21*, 1450–1472.
(38) Osikowicz, W.; de Jong, M. P.; Braun, S.; Tengstedt, C.; Fahlman, M.; Salaneck, W. R. *Appl. Phys. Lett.* **2006**, *88*, 193504:1–3.
(39) Huang, J.; Xu, Z.; Yang, Y. *Adv. Funct. Mater.* **2007**, *17*, 1966–1973.
(40) Greczynski, G.; Fahlman, M.; Salaneck, W. R. *J. Chem. Phys.* **2011**, *114*, 8628–8636.
(41) Wu, C.-I.; Lin, C.-T.; Chen, Y.-H.; Chen, M.-H.; Lu, Y.-J.; Wu, C.-C. *Appl. Phys. Lett.* **2006**, *88*, 152104:1–3.
(42) Liao, H.-H.; Chen, L.-M.; Xu, Z.; Li, G.; Yang, Y. *Appl. Phys. Lett.* **2008**, *92*, 173303:1–3.
(43) Bao, Z.; Locklin, J. *Organic Field-Effect Transistors*; CRC Press: New York, 2007.
(44) Baeg, K.-J.; Khim, D.; Kim, D.-Y.; Jung, S.-W.; Koo, J. B.; You, I.-K.; Yan, H.; Facchetti, A.; Noh, Y.-Y. *J. Polym. Sci., Part B: Polym. Phys.* **2011**, *49*, 62–67.
(45) Wu, C.-I.; Lin, C.-T.; Chen, Y.-H.; Chen, M.-H.; Lu, Y.-J.; Wu, C.-C. *Appl. Phys. Lett.* **2006**, *88*, 152104:1–3.
(46) Wei, P.; Oh, J. H.; Dong, G.; Bao, Z. *J. Am. Chem. Soc.* **2010**, *132*, 8852–8853.
(47) Zhang, Y.; de Boer, B.; Blom, P. W. M. *Phys. Rev. B* **2010**, *81*, 085201:1–5.
(48) Kim, F. S.; Guo, X.; Watson, M. D.; Jenekhe, S. A. *Adv. Mater.* **2010**, *22*, 478–482.
(49) Wei, Q.; Tajima, K.; Hashimoto, K. *ACS Appl. Mater. Interfaces* **2009**, *1*, 1865–1868.
(50) Meijer, E. J.; de Leeuw, D. M.; Setayesh, S.; van Veenendaal, E.; Huisman, B.-H.; Blom, P. W. M.; Hummelen, J. C.; Scherf, U.; Klapwijk, T. M. *Nat. Mater.* **2003**, *2*, 678–682.
(51) Zhang, X.-H.; Potscavage, W. J., Jr.; Choi, S.; Kippelen, B. *Appl. Phys. Lett.* **2009**, *94*, 043312:1–3.
(52) Sze, S. M.; Ng, K. K. *Physics of Semiconductor Devices*, 3rd ed.; Wiely-Interscience: New York, 2007.